Microelectronics Reliability 70 (2017) 32–40

Contents lists available at ScienceDirect

Microelectronics Reliability

journal homepage: www.elsevier.com/locate/microrel

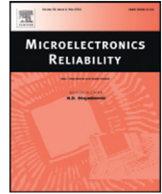

Erosion defect formation in Ni-gate AlGaN/GaN high electron mobility transistors

P.G. Whiting [a,*], M.R. Holzworth [a], A.G. Lind [a], S.J. Pearton [a], K.S. Jones [a], L. Liu [b], T.S. Kang [b], F. Ren [b], Y. Xin [c]

[a] Department of Materials Science and Engineering, University of Florida, Gainesville, FL 32611-6400, United States
[b] Department of Chemical Engineering, University of Florida, Gainesville, FL 32611-6005, United States
[c] National High Magnetic Field Lab, Florida State University, Tallahassee, FL 32310, United States

ARTICLE INFO

Article history:
Received 25 June 2014
Received in revised form 26 November 2016
Accepted 12 January 2017
Available online 29 January 2017

ABSTRACT

High electron mobility transistors based on Aluminum Gallium Nitride/Gallium Nitride heterostructures are poised to become the technology of choice for a wide variety of high frequency and high power applications. Their reliability in the field, particularly the reliability of the gate electrode under high reverse bias, remains an ongoing concern, however. Rapid increases in gate leakage current have been observed in devices which have undergone off-state stressing. Scanning Electron Microscopy, scanning probe microscopy, and Transmission Electron Microscopy have been used to evaluate physical changes to the structure of Ni-gated devices as the gate leakage current begins its initial increase. This evaluation indicates the formation of an interfacial defect similar to erosion under the gate observed by other authors. Defect formation appears to be dependent upon electrical field as well as temperature. Transmission Electron Microscopy has been used to demonstrate that a chemical change to the interfacial oxynitride layer present between the semiconductor and gate metal appears to occur during the formation of this defect. The interfacial layer under the gate contact transitions from a mixed oxynitride comprised of gallium and aluminum to an aluminum oxide.

© 2017 Elsevier Ltd. All rights reserved.

1. Introduction

High electron mobility transistors based on Aluminum Gallium Nitride/Gallium Nitride heterostructures (AlGaN/GaN HEMTs) are becoming a widely accepted semiconductor technology in telecommunications and aerospace applications [1]. This is due to the high breakdown voltages [2] and high Two Dimensional Electron Gas (2DEG) saturation velocities [3] utilized by heterostructures employed from this materials system. Despite the inherent benefits associated with this technology, many technical challenges must be surmounted if it is to be widely utilized in power and RF applications. Chief among these hurdles are the wide variety of reliability issues associated with the operation of these devices in the field [4,5].

In cases where operation requires high fields between the drain contact and the gate contact, the gate is prone to degradation. This results in undesirable increases in gate current (I_G) as well as decreases in the drain current passing between the source and drain electrodes (I_{DS}). This degradation has been observed by various researchers with different gate metal stacks [5,6,7]. Initial studies of the degradation of the gate contact began with Pt-gated devices, where many authors observed that both recoverable and non-recoverable decreases in I_{DS} resulted from electrostatic stressing of devices where large fields were applied under the gate electrode of the device under stress. Reversible electrostatic degradation effects were attributed to deep level trapping [8]. Non-recoverable increases in the gate leakage current also resulted from these stressing experiments [9].

A variety of sources of non-recoverable degradation have been observed in AlGaN/GaN HEMTs. Ivo et al. observed that interactions between electrodes from the gate electrode and unpassivated surfaces surrounding the gate contact can result in the formation of a "punchthrough"-like defect under the 2DEG. This occurs during off-state stressing when high electric fields are applied between the gate and drain electrodes of the device, resulting in degradation in I_{DS} without any increase in I_G [10]. Kawanago et al. observed that I_{DS} can also be reduced during off-state stressing without any increase in I_G due to interactions between the gate metal of the device and the AlGaN, resulting in the formation electron traps which act as a source of coulombic repulsion [11]. The mechanism for this interaction is the outdiffusion of N from the AlGaN and into the metal of the gate contact, resulting in vacancies. This can occur even in as-formed devices [12,13] and is mitigated by the use of metal nitrides or noble metals for the gate material.

The degradation mechanism most commonly referenced and studied, however, is a combination of I_{DS} reduction and I_G enhancement. The onset of this degradation was first observed in voltage-stepped stressing experiments, where the potential between the gate electrode and drain electrodes of the device was ramped from a low to high absolute value at a set rate. One observed effect of this stepped stressing experiment was a sudden increase in I_G at a more-or-less repeatable potential, termed the critical voltage (V_{CRIT}) [14].

* Corresponding author.
E-mail address: patrick.g.whiting@intel.com (P.G. Whiting).

http://dx.doi.org/10.1016/j.microrel.2017.01.007
0026-2714/© 2017 Elsevier Ltd. All rights reserved.

This definition of V_{CRIT} assumes a mechanism which is not driven by reaction kinetics, without thermal or temporal components. It also assumes that the mechanism of I_D and I_G degradation are one and the same. AlGaN and GaN are polar crystals which manifest a large inverse piezoelectric effect [15]. The first theory for the increase in I_G invoked this inverse piezoelectric effect and attributed the increase in leakage current to a fracture event at the drain side of the gate electrode where the large electrical fields present under the gate result in large tensile strain fields. This strain field could generate a void in the AlGaN which could be filled in by the Pt gate, resulting in a short to the 2DEG. Chowdhury et al. corroborated this theory with observations of pitted features under the drain side of the gate utilizing both cross-sectional Transmission Electron Microscopy (TEM) as well as, Scanning Electron Microscopy (SEM) [16]. Makaram et al. further corroborated this theory by observing pits under the gate region of a HEMT with Scanning Probe Microscopy (SPM) [17]. Both authors correlated the formation of these defects with a reduction in I_{DS}. Bajo et al. used SPM and (Electron Beam Induced Current) to correlate the presence of pitting/cracking defects within the AlGaN under the gate contact to the presence of higher leakage currents [18]. Narita et al. were able to correlate the gate leakage current with the formation of inhomogeneous electroluminescence under a transparent ITO gate ascribed to pitting defects and dislocations [19].

As later research would show, this first-order model proved to be inaccurate. While it certainly influences defect formation, strain alone cannot be the sole cause of the electrostatic degradation observed by researchers. The amount of biaxial tensile strain induced between the gate electrode and the 2DEG as a result of electrical biasing is not sufficient to induce a fracture event within the AlGaN layer of the HEMT similar to those observed with TEM and SPM. Furthermore, the initial increase in I_G observed in stepped biasing experiments can occur even when the potential is held below V_{CRIT}, which would suggest that a device need not achieve some critical strain in order for defect formation to occur. The degradation reaction associated with increasing I_G has been ascribed to a defect percolation process [20–22].

Burnham et al. [23] and Gao et al. [24] have noted that permanent increases in I_G and decreases in I_{DS} are also highly dependent upon the ambient environment in which the device under test is being stressed. Gao et al. proposed an electrochemical model for I_G/I_{DS} degradation involving OH— and hole current via trap assisted tunneling, where the Pt gate acts as the cathode and AlGaN acts as the anode [25,26]. Wu et al. used temperature-stepped stressing to demonstrate that degradation in I_D occurs only when IG is fully degraded at a given potential and that I_D degradation proceeds with activation energy of 0.84 eV. Thus, I_{DS} and I_G degradation are related but separate phenomena which are temperature activated [27]. They also observed the same pitting described previously with SPM along with an “erosion” defect not observed in any other study which correlated strongly with large increases in the channel resistance (and associated reductions in I_{DS}) of the devices under stress [28]. They noted that this defect was present, but not fully formed, in an unstressed device, indicating that the degradation was induced by initial fabrication.

Strain is not explicitly invoked in this model. Rather, pit formation is reliant on the presence of defects which act as a seed the electrochemical reaction and associated pit growth. This does not discount strain as an initiator for defect growth, however. Lang et al. have observed that the piezoelectric strain which accompanies high electric fields can induce stacking faults between the gate and drain electrodes which would serve as the seeding defects for this growth [29]. Sun et al. were able to demonstrate through electroluminescence that defect formation serves to reduce electric field as I_G increases, which would imply that defect formation also serves to relieve the piezoelectric strain present under the gate [30]. Kuball et al. observed deep level trap formation under the gate electrode of Pt-gated HEMTs and noted that trap densities appeared to increase at a rate commensurate with a diffusion-based process originating at the gate metal [31]. They noted that this diffusion process was likely mediated by biaxial strain, proposing that high electrical fields present between the gate and drain electrodes might enhance diffusion by stretching the AlGaN lattice locally at the drain side of the gate, where the electric field was maximized.

In addition to Pt-gate devices, Ni-gate HEMTs have also garnered considerable interest as a potential solution for AlGaN/GaN based circuits. These devices are also plagued by a variety of reliability issues surrounding the gate contact. Douglas et al. observed the presence of an interfacial oxide between the Ni-gate and AlGaN of HEMTs provided by a variety of manufacturers. Holzworth et al. noted that, in HEMTs provided by a commercial manufacturer, this interfacial layer was composed primarily of AlO and NiO. GaO was absent [32]. Douglas et al. noted that this interfacial layer appeared to degrade during stepped V_{GS} stressing, resulting in an I_G increase [33]. The presence of an AlO layer under the gate electrode of the HEMT should not be surprising. Other authors have observed the preferential formation of AlO over GaO as a result of ohmic contact annealing. Higashiwaki et al. observed this using XPS, noting that AlO formation occurs readily in both O_2 and N_2 ambients, suggesting that very little oxygen is actually required in order to form this surface oxide [34]. Wang et al. observed that this same AlO layer can result in dispersion losses in HEMTs after off-state stressing which could be remedied by the utilization of oxide/nitride passivation [35].

Holzworth et al. demonstrated that Ni-gated devices undergo a similar degradation process to Pt-gated devices when a high electric field is induced between the drain and gate electrodes of the device. In a study utilizing cross-sectional Transmission Electron Microscopy (TEM) in conjunction with Electron Energy Loss Spectroscopy (EELS) and Energy Dispersive X-Ray Spectroscopy (EDS), they demonstrated the presence of Ni-Al-Ga-O based pitting defect under the gate contact in HEMTs which underwent large decreases in I_{DS} during voltage-stepped stressing [36]. This was also observed by the author using SEM [37]. Lo et al. observed that Ni-based electrodes which were annealed would react with oxygen in the ambient to form NiO-based intermetallic complexes. This occurred even in a vacuum [38]. Presumably, oxygen chemisorbed onto the sample surface was sufficient to induce the formation of NiO.

The evidence above suggests an off-state degradation mechanism for Ni-gates which is similar to Pt-gate HEMTs. A pit is formed on the drain side of the gate edge which is an intermetallic oxide. The formation of this defect results in enhanced I_G in the off state as well as a reduction in I_{DS}. Curiously, no observation of an “erosion” defect has yet been observed. To this end, a search for this defect and some effort in understanding its composition and mechanism of formation seems warranted.

2. Experimental methods

For each device studied as part of this work, a Fe-doped GaN buffer layer was grown on a 6H-SiC substrate via Metal-Organic Chemical Vapor Deposition (MOCVD) to a thickness of approximately 2.25 μm, forming a reasonably stress-free layer and trapping most crystallographic defects formed in the GaN buffer layer [39]. A ~15 nm-thick layer of $Al_{0.28}Ga_{0.72}N$ with an n-type GaN capping layer was grown on the epitaxial GaN layer via MOCVD [40]. Further details regarding semiconductor epilayer growth are described elsewhere [41–43]. Ohmic contacts consisting of Ti/Al/Ni/Au were deposited and patterned on the surface. After patterning, these contacts were annealed for 30 s at 850 °C to improve conductivity [44]. The gate contact consisted of an approximately 20 nm-thick Ni liner layer deposited directly on the n-GaN cap, followed by a thicker capping layer of Au. T-gates structures with lengths of ~100 nm were used in this work [45] in addition to traditional gates with lengths of ~1.25 μm. Finally, a 100 nm-thick SiN_x passivation layer was deposited via Plasma Enhanced Chemical Vapor Deposition (PECVD). More details regarding the device fabrication process are

described elsewhere [46]. A low-magnification, representative image of a T-gate HEMT which was analyzed as part of this study is shown in Fig. 1.

Stepped stressing was performed on three devices analyzed as part of this study, where the device was electrically biased from a potential of $V_{GS} = -10$ V to $V_{GS} = -42$ V at -1 V/min with a constant potential applied to the source and drain electrodes; $V_{DS} = 15$ V. After each minute of stressing at a given value of V_{GS}, the device was biased with $V_{DS} = 0$ V and $V_{GS} = -5$ V in order to measure the leakage current flowing through the gate electrode by treating it as a reverse-biased Schottky diode. This measurement occurred over a 1 ms timespan, so the duty cycle of stressing may be assumed to be roughly equal to 100%. All stressing and measurement of device characteristics was accomplished via the use of an HP4146C semiconductor parameter analyzer, capable of independent measurements of current and voltage on all three device contacts, and a Techtronix 370A curve tracer.

It should be noted that this scheme for off-state stressing and for parametric extraction is radically different from the methodology employed by Wu et al. as part of their study [28]. When devices underwent stressing for this study, the erosion defect was not yet known and efforts were underway to observe pitting under the Ni-gate, so many of the device parameters which would have been of more interest (such as I_{DS} extraction in the on-state, V_{TH}, R_{CH}, etc.) were not collected as part of this study.

Lamellae for cross-sectional TEM analysis were formed via dual-beam Focused Ion Beam milling (FIB)/Scanning Electron Microscopy (SEM) on a FEI DB235, where in-situ sample milling, liftout, mounting, and thinning were accomplished via the use of an Omniprobe micromanipulator formed from W. All samples were coated with a thermally evaporated C layer 200 nm thick. Organometallic Pt was used to form the 2 μm protective mask utilized during milling with a Ga ion beam. Analysis of lamellae formed via FIB/SEM was performed on a JEM-ARM200cF TEM, which was probe Cs corrected with a Gatan Quantum for EELS and EDAX for EDS.

Deprocessed samples were studied using top-down SEM on the same FEI DB235 in Ultra High Resolution (UHR) mode with the Through Lens Detector selected. They were also studied using SPM, which was performed with a Veeco Dimension 3100 SPM in tapping mode. The integral gain was set at 5.0 and proportional gain was also set at 5.0 for all testing while the photodiode amplitude setpoint was held at 350 mV in order to ensure good coupling between the AFM tip and the surface. Imaging was performed with a TESP-HAR AFM tip, available from Bruker Nanosurfaces, with a 10 nm tip diameter, a 40 N/m spring constant, and a 5:1 aspect ratio.The region studied as part of SPM analysis was the channel region of the device, represented as a 512 × 512 pixel (6.75 μm × 6.75 μm) topographic map, as measured by SPM.

Deprocessing begins with an exposure to hydrofluoric acid (HF) in the form of buffered oxide etch (BOE) with a 6:1 stoichiometric ratio of HF to Ammonium Fluoride (NH_4F). BOE etching occurred for a total of 15 min, during which time the PECVD SiN_x passivation layer was dissolved. With the SiN_x removed, the metallic electrodes could be removed to fully expose the surface of the AlGaN epitaxial layer. This was accomplished via a 96 h exposure in a ferric cyanide (FeCN)/potassium iodide (KI) etch solution, known as TFAC, which is commercially available from Transcene Company, Incorporated. The KI component of this etch solution actively attacks and dissolves any metal, except platinum, with perfect selectivity to the AlGaN layer below. No etch-related defects have been observed in the AlGaN as a result of etching with TFAC, which compares favorably from previous results using Aqua Regia to remove the metal layers [35]. A second etch in 6:1 HF:NH_4F was performed to remove residual SiN_x masked by the overhang of T-gate structures. Additional solvent treatments were used to eliminate all organic contaminants from the surface of the deprocessed devices, starting with a 2 h exposure in a 1:1 mixture of *n*-heptane and acetone, which was used to dissolve and break up the bulk of the organic film in preparation for an additional 2 h exposure in methanol. This left a pristine, but hydrophobic AlGaN surface, which was very effective at attracting dust present in the processing environment. The last step in the solvent cleaning process was a 2 h ultrasonication in water, which further cleaned the sample and also generated a hydrophilic surface ideal for imaging with SEM.

3. Results and discussion

Three separate devices were off-state stressed as part of this experiment. The first, shown in Fig. 2(a) was stressed in a fashion as to avoid any dramatic increase in I_G. This suggests that macroscopic defect formation does not play a critical role in the characteristics of the device under bias at these low voltages, and the results from plan-view SEM analysis from this stress state, as shown in Fig. 2(b), appear to corroborate this supposition. No defects were observed after deprocessing and SEM analysis of this device except for some dark spotting indicative of residual organic contamination on the surface of the sample. This matches well with previous deprocessing studies of as-fabricated devices, which demonstrated pristine sample surfaces [37]. Fig. 2(c) demonstrates that the point at which off-state I_G increases appears to be the initial point where defect formation begins, which is commensurate with previous studies. Interestingly, the defect formed in the device in this stressing regime, shown in Fig. 2(d), bears little to no resemblance to the pitting defects observed previously by Chowdhury et al., Makaram et al., and Holzworth et al. [16,17,36]. In fact, no pitting defects were observed at this stress state. The observed defect appears to have an appearance more similar to the erosion defect observed by Wu et al. [28].

This is curious, as the pitting defect has been shown to correlate with off-state I_G, whereas the erosion defect observed by Wu et al. has been shown to correlate with increases in R_{CH} and associated reductions in I_{DS} in the on-state, which occurred in their study after off-state I_G had already risen to a nearly saturated value. In this case, a defect which is morphologically similar to erosion has appeared at the onset of the increase in off-state I_{GS} during off-state stressing. Because of differences in the manner in which this device was stressed in comparison to the study performed by Wu et al., it is difficult to state definitively whether the mechanism which gave rise to this defect is fundamentally different

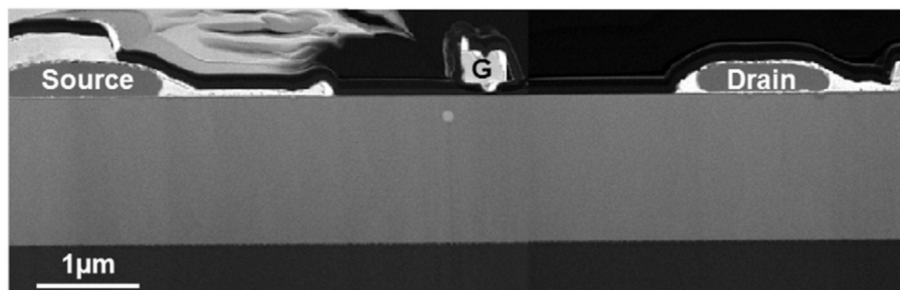

Fig. 1. A low-magnification STEM cross-section of a T-gate AlGaN/GaN HEMT.

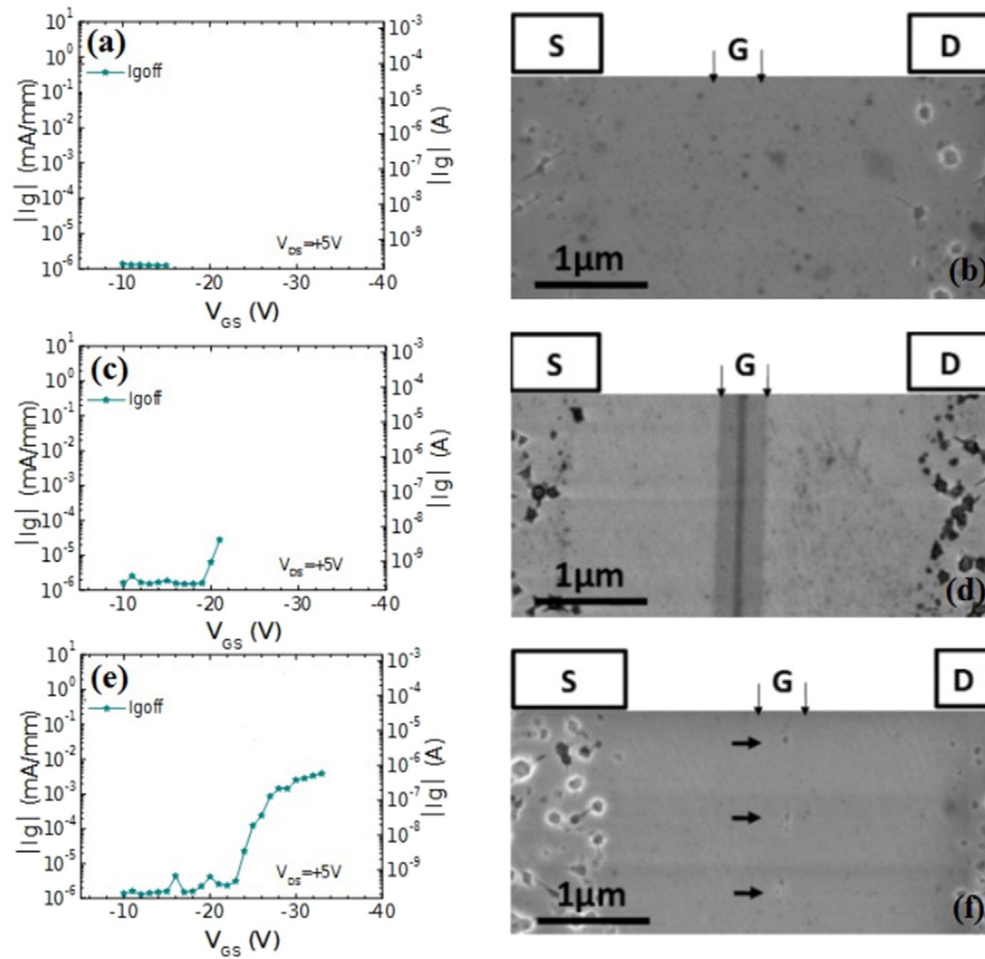

Fig. 2. a) The I_G-V_{GS} plot for an AlGaN/GaN HEMT biased such that I_G measured at $V_{GS} = -5$ V did not show a marked increase with stepped off-state stressing. (-1 V/min to $V_{GS} = -16$ V). b) Exemplary secondary electron mode SEM of the gate contact region after stressing. c) The I_G-V_{GS} plot for an AlGaN/GaN HEMT biased such that I_G measured at $V_{GS} = -5$ V showed a marked increase with stepped off-state stressing. (-1 V/min to $V_{GS} = -22$ V). d) Exemplary secondary electron mode SEM of the gate contact after stressing. e) The I_G-V_{GS} plot for an AlGaN/GaN HEMT biased such that I_G measured at $V_{GS} = -5$ V demonstrated saturation during stepped off-state stressing. (-1 V/min to $V_{GS} = -34$ V). f) Exemplary secondary electron mode SEM of the gate region of the device after stressing.

(perhaps because a Ni-gate is being degraded rather than a Pt-gate) or if it is simply being manifested in a different way because of the methodology used for degradation and parametric analysis on the HEMT itself.

In contrast to typical pitting defect formation, which might have an areal density of only a few percent in comparison to the total gate area [17,37], this defect was present along fully 66% of the gate width and along the entire gate length. It manifests itself in SEM as a dark band of contrast in the secondary electron image. This dark band of contrast is two-toned for the 100 nm gate length device. The darker toned portion of the band has a length which matches well with the length of that section of the gate which directly contacts the surface of the AlGaN epitaxial layer (approximately 100 nm, which corresponds to the neck of the "T" gate). The extent of the lighter banding to either side of this dark region matches well with the total length of the top structure of the gate electrode which does not sit in direct contact with the AlGaN epitaxial region (approximately 500 nm, corresponding to the crossbar of the "T" gate). This defect could not be removed with an additional round of the HF/TFAC based deprocessing solution. After one hour of exposure in HF, the feature was finally eliminated.

It seems plausible that the band of contrast observed in SEM is due to a thin insulating layer, insoluble in HF/TFAC, which prevents the ejection of secondary electrons out of the sample [47]. The difference in contrast may correspond to varying thickness or conductance of this insulating layer. It should be noted that this band has never been observed during the deprocessing of over 30 control samples which did not undergo any experimental treatment after being received as-fabricated. This banding defect has been observed on three separate device structures during stepped biasing where V_{DS} was non-zero. This tends to also be a condition which induces the largest increases in I_G upon initial permanent degradation.

Fig. 2(e) and Fig. 2(f) demonstrate the quality of the surface of the AlGaN epitaxial layer as a device is step stressed at -1 V/min well beyond the initial increase in I_G. As shown in this figure, the dark band of contrast observed at the initial onset of degradation is no longer visible. It is replaced by the well-documented pitting defect observed by various authors in Ni-gated devices as well as in Pt-gated devices. The pitting defect covers approximately 5.5% of the total areal density of the 100 nm gate studied as part of the experiment. A corresponding increase in the gate leakage current above that observed at initial breakdown is shown for this same device in Fig. 2(e). This increase in I_G is commensurate with the results of previous studies of the phenomenon [36,37]. There are a variety of possible explanations for why it is that the band of contrast is not present in devices stressed to high levels of off-state I_G. It is understood that extended periods of off-state stressing past initial degradation induce substantial reactivity and mobility of nickel atoms present within the liner layer of the gate electrode [36]. This influx of nickel may result in the consumption of the defect present at the interface.

Wu et al. observed previously that I_G and R_{CH} degradation, which correspond to pitting and erosion, respectively, are thermally activated

electrochemical degradation processes [27,28]. During off-state stressing, the gate is placed under a high negative potential. The electric field permeates the device underneath the entire gate length, including the raised portion which makes up the crossbar of the "T", but is maximized where the gate makes direct contact with the AlGaN. At zero bias, the gate electrode can be considered to be at a floating potential. A smaller electrostatic field present between the gate electrode and the 2DEG arises from the built-in potential (and associated dipole) generated by the difference in workfunction between the contacting gate metal and the AlGaN layer beneath it. The vertical field directly under the gate in this case is significantly reduced and is confined to the region directly under the gate, but it is non-zero. Thus, the formation of the erosion defect could also be induced by thermal annealing of a Ni-gated device, where only the built-in potential is present.

Fig. 3 demonstrates a defect with morphology similar to that of the electrically induced defect shown in Fig. 2(c), observed after deprocessing of an as-formed device annealed in a Lindberg Furnace at 500 °C for 30 min in an air ambient. This defect was present in devices with both 100 nm gate lengths, shown in Fig. 3(a), and 1.25 μm gate lengths, shown in Fig. 3(b). The morphology of this defect was the same between both annealed devices. It should be noted that electrical characterization of annealed samples to verify enhanced leakage I_G was not possible in this study because of mixing of the Ni liner and Au cap of the gate electrode.

In contrast to the results demonstrated previously during stressing of the 100 nm gate devices, the defect observed on these devices only extends over the region where the gate electrode makes direct contact with the surface of the AlGaN epilayer. The band of contrast which forms under the gate foot in an annealed device, where the only field present is due to the built-in potential between the electrode and the AlGaN, should have reacted less than the bands which form under the raised portion of the T-gate during electrostatic stressing, where the electrostatic field is much larger. This appears to be the case in comparing Fig. 2(a) with Fig. 2(d).

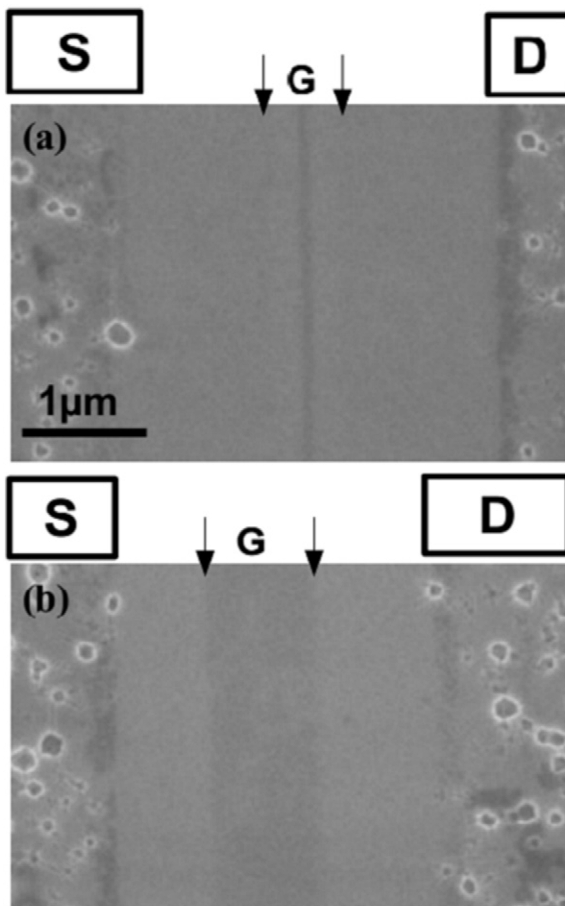

Fig. 3. a) A defect with morphological similarity to the one observed in Fig. 1(d), this one formed on a 100 nm Ni "T" gate via thermal annealing at 500 °C for 30 min as observed in secondary electron mode SEM. b) A defect with morphological similarity to the one observed in Fig. 1(d), this one formed on a 100 nm Ni "T" gate via thermal annealing at 500 °C for 30 min as observed in secondary electron mode SEM.

The observations above suggest a mechanism for defect formation which is electrochemical in nature and which is thermally activated. The electrostatic model outlined above also explains the "two toned" characteristic of the banding defect present in the electrically biased "T" gate, wherein electric fields are maximized where the gate makes direct contact with the AlGaN and reduced, but non-zero where the gate is raised away from the AlGaN surface. It should be noted that the results above also indicate that the electrochemical reaction involved in the formation of the erosion defect cannot be the same as the pitting reaction detailed by Gao et al. [25,26], because that model requires a trap assisted tunneling current of holes from the AlGaN/GaN interface. A supply of holes via trap-assisted tunneling would require electric fields much higher than those induced at the metallurgical junction between the AlGaN and Ni gate with zero bias.

SPM analysis was performed on the surface of a sample which formed the observed defect after annealing at 500 °C for 30 min. As shown in Fig. 4(a) and Fig. 4(b), the dark band of contrast which appeared in SEM, and which matched closely with the dimensions of the 1 μm Ni-gate, is still visible during SPM analysis. A 3.5 μm wide region of the channel was integrated in order to analyze the thickness of this reacted region. According to the averaged linescan resulting from this analysis, shown in Fig. 4(b), this dark band of contrast corresponds to a raised region on the surface of the AlGaN epitaxial layer possessing an average height of approximately 1.5 nm. This is a curious result when juxtaposed against the results from Wu et al. [28], where the erosion defect corresponded to a 2 nm pit under the gate contact.

The roughness of this region does not differ substantially from the roughness of the surrounding deprocessed AlGaN surface. The Root Mean Squared (RMS) roughness of the channel region was determined by means of a second measurement with SPM of a 1.5 × 1.5 μm section inside and outside of the reacted defect region within the channel. All other settings were maintained between the two measurements. Analysis of the RMS surface roughness was performed on both regions. The unreacted channel region of the device was found to have a surface roughness approximately equal to 3.7 Å while the surface roughness of the reacted region was determined to be approximately equal to 3.4 Å. Because the two observed roughness values are nearly equal, the material being formed as a result of thermal annealing is likely a contiguous layer which is a product of a reaction at the epitaxial interface between the AlGaN and the Ni.

Fig. 4(c) shows the results of isochronal annealing and subsequent deprocessing of devices for 30 min at variable temperatures ranging from 350 °C to 550 °C in 25 °C steps. Analysis was performed on the channel regions of a group of 1 μm gate length devices via SPM over a 3 μm × 2 μm area. The resulting averaged step height between the banded region under the gate and the channel region itself was obtained. The standard deviation associated with the variable height within the banded region versus within the channel is depicted in the error bars contained within this figure, and matches reasonably well with the RMS surface roughness observed previously. The isochronal annealing sequence described previously shows that the banded feature observed under the gate region of the device begins to form at approximately 425 °C and is a fully formed feature, which does not appear to grow appreciably larger than 1.5 nm by 475 °C.

In order to explain the mechanism of formation for this defective region at the AlGaN interface, information about its composition was obtained via cross-sectional TEM analysis. A control sample was formed from a device which was received as-fabricated and a second sample was formed from a device which was annealed at 500 °C for 30 min,

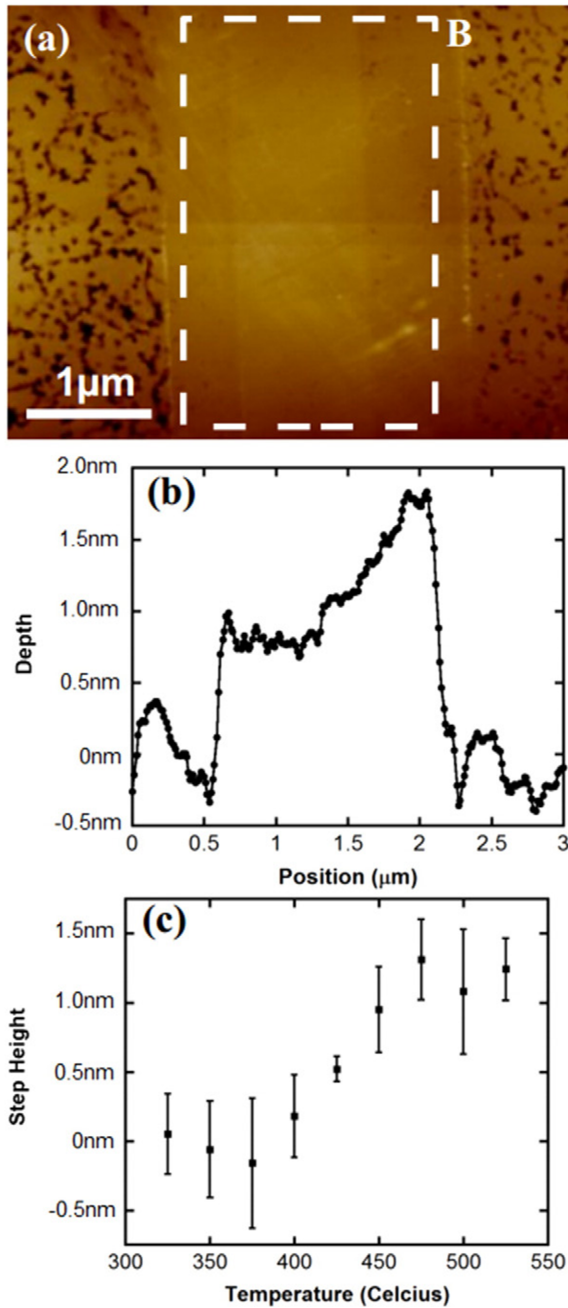

Fig. 4. a) A representative 3.5 μm × 6.5 μm areal scan performed via SPM on the channel region of a HEMT which was thermally annealed at 500 °C for 30 min. The dashed boxed indicates the area from which the SPM data was used to form a representative averaged linescan, shown in Fig. 3(b). Lighter regions indicate higher altitudes while darker regions indicate lower altitudes. b) An averaged linescan, per Fig. 3(a). c) Analysis with SPM of 3 μm × 2 μm aerial scans of the channel regions of devices annealed from 350 °C to 550 °C and deprocessed.

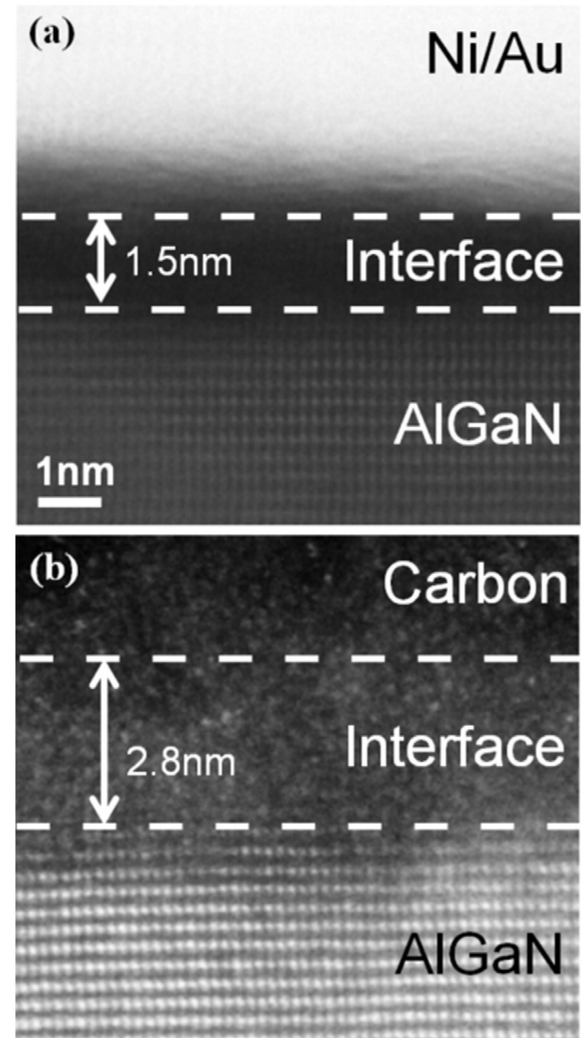

Fig. 5. a) STEM HAADF images performed on a control sample formed via FIB/SEM cross-sectioning from an as-fabricated AlGaN/GaN HEMT. b) STEM HAADF performed on a sample formed via FIB/SEM cross-sectioning from an AlGaN/GaN HEMT which was chemically deprocessed and carbon-coated after annealing for 30 min at 500 °C.

the same condition used to produce the defect shown in Fig. 2 and Fig. 3. Fiduciary marks which set off the gate region of the device were added to both samples to ensure that the lamellae formed captured the surface under the gate electrode of each device.

As shown in Fig. 5(a) and Fig. 6(a), atomic resolution high angle annular dark field STEM (STEM HAADF) images and high resolution TEM (HRTEM) analysis of the control device demonstrate the presence of an interfacial layer between the AlGaN surface of the HEMT device and the nickel gate of this device, which has been observed in previous studies using APT [21]. This interfacial layer remained after annealing, deprocessing, carbon coating, and FIB cross-sectioning, as shown in Fig. 5(b) and Fig. 6(b). Reaction by means of thermal annealing or electrostatic biasing appears to induce some sort of chemical change within this interfacial layer which makes it much less pervious to the etch chemistries used for sample preparation in plan-view SEM.

From the STEM HAADF images of Fig. 5(a) and Fig. 5(b), it is easy to locate the first atomic AlGaN layer above which the interface layer starts. The thickness of this interfacial layer is approximately 1.5 nm prior to annealing and deprocessing, as shown in Fig. 5(a), and approximately 2.8 nm after annealing and deprocessing, as shown in Fig. 5(b). Given that SPM measurements indicated that this layer rises above the surrounding AlGaN by only 1.5 nm after annealing, the results from STEM would suggest that some consumption of the underlying AlGaN layer occurs as the interface undergoes reaction as part of defect formation under the gate contact. If the interfacial layer was removed and imaged with SPM, this would result in a pit similar in depth to the erosion defect observed by Wu et al. [28].

Analysis of HRTEM images of the interfacial layer by Fast Fourier Transform (FFT processed with Image J® software) suggests that this region is amorphous in nature both before and after the formation of the defect present under the gate. The array of bright spots in the FFT, are dim and match closely with the positioning of spots in the FFT of the underlying AlGaN layer. This indicates that the observed dim spots in the FFT of the interface do not arise from a unique crystalline phases within

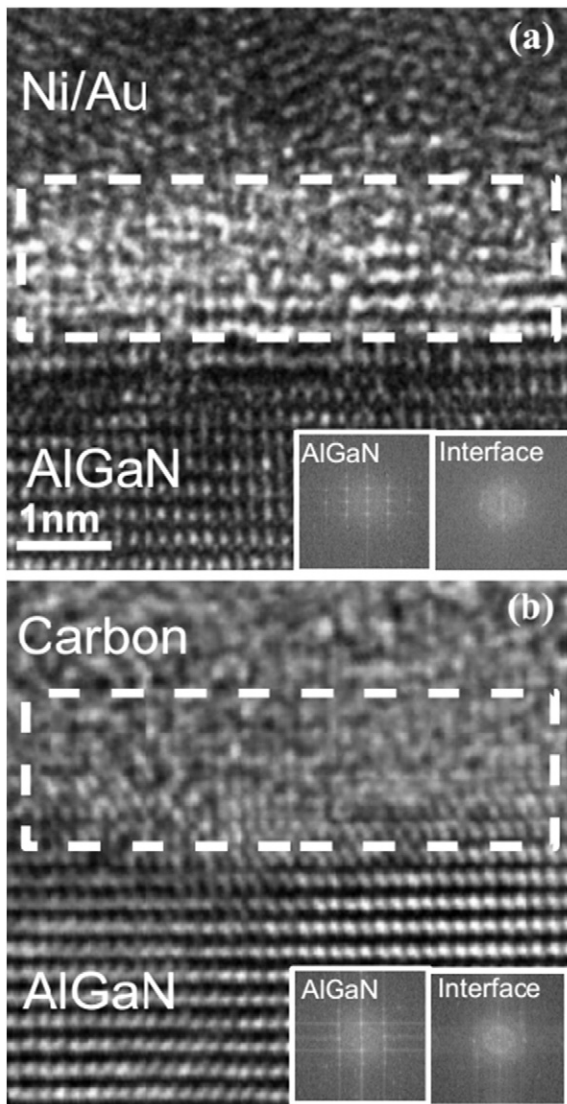

Fig. 6. a) HRTEM performed on a control sample formed via FIB/SEM cross-sectioning from an as-fabricated AlGaN/GaN HEMT. Insets are the FFT from AlGaN and interfacial layer. b) HRTEM performed on a sample formed via FIB/SEM cross-sectioning from an AlGaN/GaN HEMT which was deprocessed and carbon-coated after annealing for 30 min at 500 °C. Insets are the FFT from AlGaN and interfacial layer.

this layer, but are more likely induced by a thickness effect within the cross-sections.

In order to determine the chemical composition of the interfacial layer, STEM EELS mapping and STEM EDS linescans were performed with a probe size of 1.1 Å. As shown in Fig. 7(a) and Fig. 7(b), STEM EELS mapping reveals that this interfacial layer is oxygen-rich in comparison to the surrounding AlGaN regions and that this remains the case both before and after annealing/deprocessing of the device structure. The EELS signal arising from N is present in this interfacial layer in the control sample, as shown in Fig. 7(a), suggesting that the interfacial layer is an oxynitride prior to annealing, commensurate with studies of annealed and unpassivated AlGaN, which are similar the condition of the AlGaN in this study after the formation of ohmic contacts [34]. Upon annealing, the signal arising from N in this layer is greatly diminished, as is shown in Fig. 7(b). This suggests that, after annealing, the native oxynitride which is present on the surface of the AlGaN reforms and undergoes some chemical reaction which converts it to an oxide, nearly completely rejecting N. Ga out-diffusion also appears to occur.

In order to ascertain more information about the chemical structure of this native oxynitride and its conversion to an oxide upon annealing, a STEM EDS linescan was performed. EDS was chosen as a complementary technique to EELS because the Al peak is obscured by the tail of the Ga peak in the EELS spectrum. Fig. 8 shows the EDS spectra associated with a STEM linescan across the interfacial layer in samples formed both before (Fig. 8(a)) and after (Fig. 8(b)) thermal annealing at 500 °C for 30 min of the HEMT device structure. Three general regions of interest are contained within each of these EDS linescans, those being the AlGaN layer (dominated by Al Kα and Ga Kα), the Nickel liner layer (dominated by Ni Kα and interdiffused Au Lα) and the interfacial region (coinciding with the slight increase in the EDS signal arising from the O Kα peak). The EDS linescan shown in Fig. 8(b) demonstrates that, upon annealing at 500 °C for 30 min, a peak in the Al Kα EDS signal forms within the interfacial layer. This result is consistent over a range of different analyzed regions and is consistent from one annealed sample to another. This suggests that, during this electrochemical degradation process, the interfacial region between the AlGaN and Ni-gate is undergoing a conversion from an intermetallic compound, formed from mixed Al, Ga, O, and N, to an AlO-based compound which rejects N and getters Al.

The formation of this aluminum oxide-based interfacial layer could cause the increase in leakage observed at the gate contact. It bears noting that the thickness associated with maximum conduction of an Al contact to GaAs with an Al_2O_3 interfacial layer, thanks to the interplay of dipole formation and tunneling resistance, is approximately 1.5 nm [48], which is comparable to the thickness of the insulating layer

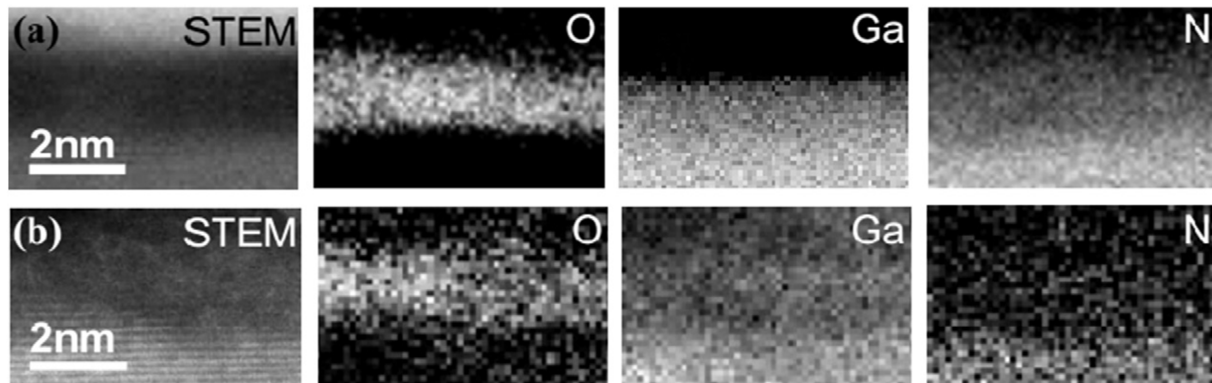

Fig. 7. a) STEM EELS mapping performed on a control sample formed via FIB/SEM cross-sectioning from an as-fabricated AlGaN/GaN HEMT. b) STEM EELS mapping performed on a sample formed via FIB/SEM cross-sectioning from an AlGaN/GaN HEMT which was deprocessed and carbon-coated after annealing for 30 min at 500 °C.

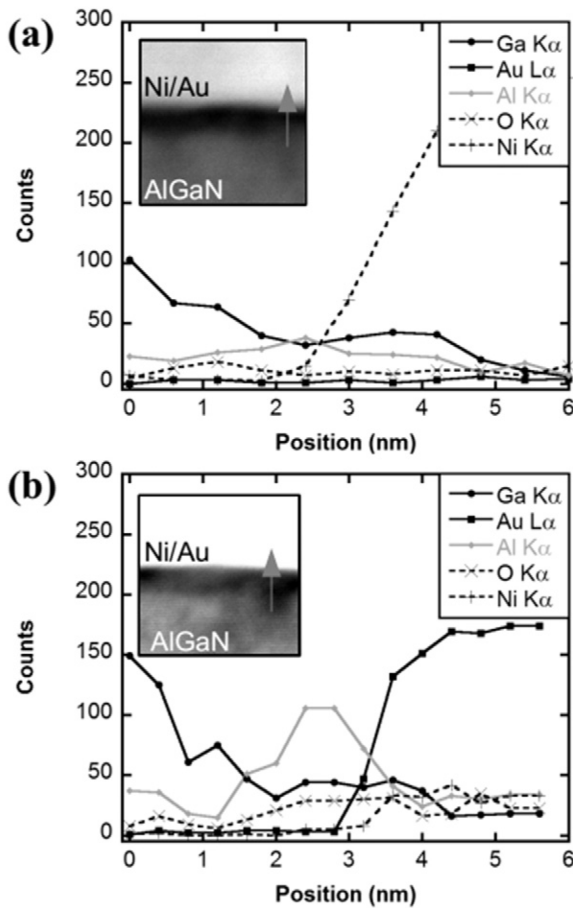

Fig. 8. a) An EDS linescan performed over the AlGaN/Ni-Gate interface of a control sample formed via FIB/SEM cross-sectioning from an as-fabricated. Inset represents the regions over which the linescans were taken with the arrow indicating the direction of each linescan. b) An EDS linescan performed over the AlGaN/Ni-Gate interface of a sample formed via FIB/SEM cross-sectioning from a HEMT which was deprocessed and carbon-coated after annealing for 30 min at 500 °C. Inset represents the regions over which the linescans were taken with the arrow indicating the direction of each linescan.

observed with TEM. However, this same relationship has not been explicitly been demonstrated for AlN/GaN materials and the critical thickness for this conduction mechanism may differ significantly.

4. Conclusion

Off-State stressing performed on an AlGaN/GaN HEMT with a Ni gate has resulted in the formation of an interfacial defect under the gate contact of the device which manifests itself when IG initially increases during −1 V/min V_{GS} stressing with V_{DS} held constant. SEM/SPM of off-state stressed and annealed devices have demonstrated that the reaction which forms this defect is electrochemical in nature and is modulated by electric field and by temperature, resulting in a band of dark contrast in SEM and a corresponding raised feature in AFM. EDS/EELS analyses via STEM as well as HRTEM have shown that this interfacial defect is an amorphous layer of AlO which is formed from the rejection of N and the consumption of Al from an as-formed interfacial layer composed of Al, Ga, O, and N. This results in the formation of a 2.8 nm thick insulating layer between the AlGaN and Ni-gate which consumes approximately 1.3 nm of underlying AlGaN during its formation. This effect has not been observed previously during annealing studies of AlGaN, wherein oxynitride formation and not oxide formation has been observed, and appears to be the district hallmark of the electrochemical degradation process which causes defect formation under the Ni-gate contact.

The defect described above is similar morphologically to erosion defects observed by Wu et al. [28]. While those authors observed the formation of a pit under the gate contact of the device via SPM, however, this study has demonstrated a raised region via SPM. This discrepancy may be caused by the use of TFAC etchant for deprocessing, which is benign to AlO compounds, instead of Aqua Regia, which has a non-zero etch rate on some forms of AlO [49]. The defect itself does not appear to impact device characteristics in the same fashion as the erosion defect observed by Wu. This could be caused by the −1 V/min ramped off-state stressing of the device, which was quite different from the methodology used by Wu, or by the use of Ni for the gate contact rather than Pt, which seemed to interact with the interfacial defect as I_G continued to increase during off-state stressing. The authors expect that the use of MIS-HEMT technology and the associated intentional generation of an interfacial oxide present between the gate contact and the AlGaN epilayer [50] will mitigate the formation of this defect, though reliability of these novel devices is an open question in and of itself [51].

References

[1] E.O. Johnson, Physical limitation on frequency and power parameters of transistors, RCA Rev. (1965) 163–176.
[2] S.T. Sheppard, K. Doverspike, W.L. Pribble, S.T. Allen, J.W. Palmour, L.T. Kehias, T.J. Jenkins, High-power microwave GaN/AlGaN HEMTs on semi-insulating silicon carbide substrates, IEEE Electon Device Lett. 20 (1999) 161–163.
[3] M. Feng, S.C. Shen, D.C. Caruth, J.J. Huang, Device technologies for RF front-end circuits in next-generation wireless communications, Proc. IEEE 92 (2004) 354–375.
[4] G. Menghesso, Reliability of GaN high-electron-mobility transistors: state of the art and perspectives, IEEE Trans. Device Mater. Reliab. 8 (2008) 332–344.
[5] J. DelAlamo, J. Joh, GaN HEMT reliability, Microelectron. Reliab. 49 (2009) 1200–1206.
[6] C.Y. Chang, T. Anderson, J. Hite, L. Lu, C.F. Lo, B.H. Chu, D.J. Cheney, E.A. Douglas, B.P. Gila, F. Ren, G.D. Via, P. Whiting, R. Holzworth, K.S. Jones, S. Jang, S.J. Pearton, Reverse gate bias-induced degradation of AlGaN/GaN high electron mobility transistors, Vac. Sci. Technol. B 28 (2010) 1044.
[7] L. Liu, C.F. Lo, T.S. Kang, S.J. Pearton, I.I. Kravchenko, O. Laboutin, Y. Cao, J.W. Johnson, F. Ren, Comparison of DC performance of Pt/Ti/Au and Ni/Au gated AlGaN/GaN HEMTs, J. Vac. Sci.Technol. B 29 (2011) 042202.
[8] J. Joh, J.A. del Alamo, Impact of electrical degradation on trapping characteristics of GaN high electron mobility transistors, IEEE IEDM Tech. Dig. 461-464 (2008).
[9] J. Joh, L. Xia, J.A. del Alamo, Gate current degradation mechanisms of GaN high electron mobility transistors, IEEE IEDM Tech. Dig. (2007) 385–388.
[10] P. Ivo, P. Kotara, L. Schellhase, R. Lossy, U. Zeimer, A. Mogilatenko, J. Wurfl, G. Trankle, A. Glowacki, C. Boit, New degradation mechanism observed for AlGaN/GaN HEMTs with sub 100 nm scale unpassivated regions around the gate periphery, Microelectron. Reliab. 54 (2014) 1288–1292.
[11] T. Kawanago, K. Kakushima, Y. Kataoka, A. Nishiyama, N. Sugii, H. Wakabayashi, K. Tsutsui, K. Natori, H. Iwai, Gate technology contributions to collapse of drain current in AlGaN/GaN Schottky HEMT, Trans. Electron Device 61–3 (2014) 785–792.
[12] R.S. Kajen, L.K. Bera, H.R. Tan, S.B. Dolmanan, Z.W. Cheong, S. Tripathy, Formation of Ni diffusion-induced surface traps in GaN/$Al_xGa_{1-x}N$/GaN heterostructures on silicon substrate during gate metal deposition, J. Electron. Mater. 45-1 (2015) 493–498.
[13] M. Meneghini, M. Bertin, A. Stocco, G. dal Santo, D. Marcon, P.E. Malinowski, A. Chini, G. Meneghesso, E. Zanoni, Degradation of AlGaN/GaN Schottky diodes on silicon: Role of defects at the AlGaN/GaN interface, Appl. Phys. Lett. 102 (2013) 163501.
[14] J. Joh, J.A. del Alamo, Critical voltage for electrical degradation of GaN highelectron mobility transistors, IEEE Electron Device Lett. 29 (2008) 287–289.
[15] F. Bemardini, V. Fiorentini, D. Vanderbilt, Spontaneous polarization and piezoelectric constants of III-V nitrides, Phys. Rev. B 56 (1997).
[16] U. Chowdhury, J.L. Jimenez, C. Lee, E. Beam, P. Saunier, T. Balistreri, TEM observation of crack- and pit-shaped defects in electrically degraded GaN HEMTs, IEEE Electron Device Lett. 29 (2008) 1098–1100.
[17] P. Makaram, J. Joh, J.A. del Alamo, T. Palacios, C.V. Thompson, Evolution of structural defects associated with electrical degradation in AlGaN/GaN high electron mobility transistors, Appl. Phys. Lett. 96 (2010) 233591.
[18] M.M. Bajo, C. Hodges, M.J. Uren, M. Kuball, On the link between electroluminescence, gate current leakage, and surface defects in AlGaN/GaN high electron mobility transistors upon off-state stress, Appl. Phys. Lett. 101 (2012) 033508.
[19] T. Narita, Y. Fujimoto, A. Wakejima, T. Egawa, Identification of local gate leakage with electroluminescence using AlGaN/GaN HEMTs, Electron. Lett. 50-16 (2014) 1162–1164.
[20] M. Meneghini, A. Stocco, M. Bertin, D. Marcon, A. Chini, A. Meneghesso, E. Zanoni, Time-dependent degradation of AlGaN/GaN high electron mobility transistors under reverse bias, Appl. Phys. Lett. 100 (2012) 033505.
[21] P. Marko, A. Alexewicz, O. Hilt, G. Meneghesso, E. Zanoni, J. Wurfl, G. Strasser, D. Pogany, Random telegraph signal noise in gate current of unstressed and reverse-bias-stressed AlGaN/GaN high electron mobility transistors, Appl. Phys. Lett. 100 (2012) 143507.

[22] A. Chini, M. Esposto, G. Meneghesso, E. Zanoni, Evaluation of GaN HEMT degradation by means of pulsed I-V, leakage and DLTS measurements, IEEE Electron. Lett. 45 (2009) 426–442.
[23] S.D. Burnham, R. Bowen, P. Willadsen, H. Bracamontes, P. Hashimoto, M. Hu, D. Wong, M. Chen, M. Microvic, Reliability of T-gate AlGaN/GaN HEMTs, Phys. Status Solidi C 8 (2011) 2399–2403.
[24] F. Gao, B. Lu, L. Li, S. Kaun, J.S. Speck, C.V. Thompson, T. Palacios, Role of oxygen in the OFF-state degradation of AlGaN/GaN high electron mobility transistors, Appl. Phys. Lett. 99 (2011) 223506.
[25] F. Gao, C.V. Thompson, J.A. del Alamo, T. Palacios, Role of electrochemical reactions in the degradation mechanisms of AlGaN/GaN HEMTs, CS MANTECH, 63, 2014.
[26] F. Gao, S.C. Tan, J.A. del Alamo, C.V. Thompson, T. Palacios, Impact of electrochemical reactions on the OFF-state degradation of AlGaN/GaN HEMTs, IEEE Trans. Electron Device 61–2 (2014) 437–444.
[27] Y. Wu, C.-Y. Chen, J.A. del Alamo, Activation energy of drain-current degradation in GaN HEMTs under high-power DC stress, Microelectron. Reliab. 54-12 (2014) 2668–2674.
[28] Y. Wu, C.Y. Chen, J.A. del Alamo, Electrical and structural degradation of GaN HEMTs under high-power and high-temperature DC stress, J. Appl. Phys. 117-2 (2015) 025707.
[29] A.C. Lang, J.L. Hart, J.G. Wen, D.J. Miller, D.J. Meyer, M.L. Taheri, I2 basal stacking fault as a degradation mechanism in reverse gate-biased AlGaN/GaN HEMTs, Appl. Phys. Lett. 109 (2016) 133509.
[30] M. Sun, M. Montes Bajo, M.J. Uren, M. Kuball, Implications of gate-edge electric field in AlGaN/GaN high electron mobility transistors during OFF-state degradation, Microelectron. Reliab. 54-12 (2014) 2650–2655.
[31] M. Kuball, M. Tapajna, R.J.T. Simms, M. Faqir, U.K. Mishra, AlGaN/GaN HEMT device reliability and degradation evolution: importance of diffusion processes, Microelectron. Reliab. 5 (2010) 195–200.
[32] M.R. Holzworth, N. Rudawski, S.J. Pearton, K.S. Jones, L. Lu, T.S. Kang, F. Ren, J.W. Johnson, Characterization of the gate oxide of an AlGaN/GaN HEMT, Appl. Phys. Lett. 98 (2011) 122103.
[33] E.A. Douglas, C.Y. Chang, D.J. Cheney, B.P. Gila, C.F. Lo, L. Liu, R. Holzworth, P. Whiting, K.S. Jones, G.D. Via, J. Kim, S. Jang, F. Ren, S.J. Pearton, AlGaN/GaN high electron mobility transistor degradation under on- and off-state stress, Microelectron. Reliab. 51 (2011) 207.
[34] M. Higashiwaki, S. Chowdhury, B.L. Swenson, U.K. Mishra, Effects of oxidation on surface chemical states and barrier height of AlGaN/GaN heterostructures, Appl. Phys. Lett. 97 (2010) 222104.
[35] R. Wang, G. Li, J. Guo, B. Song, J. Verma, Z. Hu, Y. Yue, K. Nomoto, S. Ganguly, S. Rouvimov, X. Gao, O. Laboutin, Y. Cao, W. Johnson, P. Fay, D. Jena, H.G. Xing, Dispersion-free operation in InAlN-based HEMTs with ultrathin or no passivation, Electron Devices Meeting, IEEE '13 International, 2013, pp. 703–706.
[36] M.R. Holzworth, N.G. Rudawski, P.G. Whiting, S.J. Pearton, K.S. Jones, L. Lu, T.S. Kang, F. Ren, E. Patrick, M.E. Law, Field-induced defect morphology in Ni-gate AlGaN/GaN high electron mobility transistors, Appl. Phys. Lett. 103 (2013) 023503.
[37] P.G. Whiting, N.G. Rudawski, M.R. Holzworth, S.J. Pearton, K.S. Jones, L. Liu, T.S. Kang, F. Ren, Under-gate defect formation in Ni-gate AlGaN/GaN high electron moblity transistors, Microelectron. Reliab. 52 (2012) 2542–2546.
[38] C.F. Lo, L. Liu, T.S. Kang, R. Davies, B.P. Gila, S.J. Pearton, I.I. Kravchenko, O. Laboutin, Y. Cao, W.J. Johnson, F. Ren, Improvement of off-state stress critical voltage by using Pt-gated AlGaN/GaN High Electron Mobility Transistors, Electrochem. Sol. State Lett. 14 (2011) H264–H267.
[39] S. Kolluri, S. Keller, S.P. DenBaars, U.K. Mishra, Microwave power performance n-polar GaN MISHEMTs grown by MOCVD on SiC substrates using an Al_2O_3 etch-stop technology, IEEE Electron Device Lett 33 (2012) 44–46.
[40] M.A. Khan, J.N. Kuznia, J.M. Vanhove, D.T. Olson, S. Krishnankutty, R.M. Kolbas, Growth of high optical and electrical quality GaN layers using low-pressure metalorganic chemical vapor-deposition, Appl. Phys. Lett. 58 (1991) 526–527.
[41] W. Nagy, J. Brown, R. Borges, S. Singhal, Linearity characteristics of microwave-power GaN HEMTs, IEEE Trans. Microwave Theory Tech. 51 (2003) 660–664.
[42] S. Singhal, T. Li, A. Chaudhari, A.W. Hanson, R. Therrien, J.W. Johnson, et al., Reliability of large periphery GaN-on-Si HFETs, Microelectron. Reliab. 46 (2006) 1247–1253.
[43] J.D. Brown, R. Borges, E. Piner, A. Vescan, S. Singhal, R. Therrien, AlGaN/GaN HFETs fabricated on 100-mm GaN on silicon (111) substrates, Solid State Electron. 46 (2002) 1535–1539.
[44] Luo B, Kim J, Mehandru R, Ren F, Lee KP, Pearton SJ, et al. Comparison of ohmic contact properties on n-GaN/p-SiC and n-AlGaN/p-SiC heterojunctions. Solid State Electron.
[45] W.-K. Wang, P.-C. Lin, C.-H. Lin, C.-K. Lin, Y.-J. Chan, G.-T. Chen, et al., Performance enhancement by using the n^{+}-GaN cap layer and gate recess technology on the AlGaN-GaN HEMT fabrication, IEEE Electron Device Lett. 26 (2005) 5–7.
[46] E.A. Douglas, C.Y. Chang, B.P. Gila, M.R. Holzworth, K.S. Jones, L. Liu, et al., Investigation of the effects of temperature during off-state degradation of AlGaN/GaN high electron mobility transistors, Microelectron. Reliab. 52 (2012) 23–28.
[47] J. Goldstein, D.E. Newberry, Electron beam – specimen interactions, Scanning Electron Microscopy and X-ray Microanalysis, Kulwer Academic/Plenum Publishers, New York 2003, pp. 61–97.
[48] J. Hu, K.C. Saraswat, H.S.P. Wong, Metal/III-V schottky barrier height tuning for the design of non-alloyed field effect transistor source/drain contacts, J. Appl. Phys. 107 (2010) 06712.
[49] K.R. Williams, K. Gupta, Etch rates for micromachining processing—part II, J. Microelectromech. Syst. 12–6 (2003) 761–778.
[50] J. Chen, T. Kawanago, H. Wakabayashi, K. Tsutsui, H. Iwai, D. Nohata, H. Nohira, K. Kakushima, La_2O_3 gate dielectrics for AlGaN/GaN HEMT, Microelectron. Reliab. 60 (2016) 16–19.
[51] S. Warnock, J.A. del Alamo, Progressive breakdown in high-voltage GaN MIS-HEMTs, Reliability Physics Symposium, IEEE '16. International;2016.4A-6, 2016.